Cross-section measurements of (n, $2n$) and (n, p) reactions on ^{124,126,128,130,131,132}Xe in the 14 MeV region and theoretical calculations of their excitation functions*

Junhua Luo(罗均华)[1,2†] Li Jiang(蒋励)[3] Juncheng Liang(梁珺成)[4] Fei Tuo(拓飞)[5]
Long He(贺龙)[1] Liang Zhou(周亮)[2]

[1]Institute of New Energy, Hexi University, Zhangye 734000, China
[2]School of Physics and Electromechanical Engineering, Hexi University, Zhangye 734000, China
[3]Institute of Nuclear Physics and Chemistry, China Academy of Engineering Physics, Mianyang 621900, China
[4]National Institute of Metrology, Beijing 100029, China
[5]National Institute for Radiological Protection, China CDC, Beijing 100088, China

Abstract: The reaction cross-sections of ^{124}Xe(n, $2n$)^{123}Xe, ^{126}Xe(n, $2n$)^{125}Xe, ^{128}Xe(n, $2n$)^{127}Xe, ^{130}Xe(n, $2n$)^{129m}Xe, ^{132}Xe(n, $2n$)^{131m}Xe, ^{130}Xe(n, p)^{130}I, ^{131}Xe(n, p)^{131}I, and ^{132}Xe(n, p)^{132}I were measured at the 13.5, 13.8, 14.1, 14.4, and 14.8 MeV neutron energies. The monoenergetic neutrons were generated via the ^{3}H(d,n)^{4}He reaction at the China Academy of Engineering Physics using the K-400 Neutron Generator with a solid ^{3}H-Ti target. A high-purity germanium detector was employed to measure the activities of the product. The reactions ^{93}Nb(n, $2n$)^{92m}Nb and ^{27}Al(n, α)^{24}Na were adopted for neutron flux calibration. The cross sections of the (n, $2n$) and (n, p) reactions of the xenon isotopes were obtained within the 13–15 MeV neutron energy range. These cross-sections were then compared with the IAEA-exchange format (EXFOR) database-derived experimental data, together with the evaluation results of the CENDL-3, ENDF/B-VIII.0, JENDL-4.0, RUSFOND, and JEFF-3.3 data libraries, as well as the theoretical excitation function obtained using the TALYS-1.95 code. The cross-sections of the reactions (except for the ^{124}Xe(n, $2n$)^{123}Xe and ^{132}Xe(n, p)^{132}I) at 13.5, 13.8, and 14.1 MeV are reported for the first time in this study. The obtained results are beneficial in providing better cross-section constraints for the reactions in the 13–15 MeV region, thus improving the quality of the corresponding database. Meanwhile, these data can also be used for the verification of relevant nuclear reaction model parameters.

Keywords: ^{124,126,128,130,131,132}Xe isotopes, 14 MeV neutrons, (n, $2n$) and (n, p) reactions, Excitation function, TALYS-1.95 code

DOI: 10.1088/1674-1137/ac3fa4

I. INTRODUCTION

Xenon is a natural element with the atomic number $Z = 54$. It has nine stable isotopes with Z numbers following that of tin. Its isotopes are ^{126}Xe(0.0890%), ^{124}Xe(0.0952%), ^{128}Xe(1.9102%), ^{130}Xe(4.0710%), ^{136}Xe(8.8573%), ^{134}Xe(10.4357%), ^{131}Xe(21.232%), ^{129}Xe(26.4006%), and ^{132}Xe(26.9086%) [1]. These isotopes are prominent in the study of nuclear energy and nuclear physics. First, xenon is ideal for studying plasma conditions at high temperatures and pressure owing to its remarkable physical properties. In the design of a fusion reactor, adding an appropriate xenon gas and harnessing its pressure resistance and thermal neutron absorption characteristics can effectively prevent nuclear leakages, thereby ensuring the safety of nuclear reactors such as the international thermonuclear experimental reactor (ITER) and accelerator-driven subcritical systems (ADSs) [2]. The ^{3}H(d,n)^{4}He fusion could provide output energy up to 14 MeV. In this case, the neutron yields would be (5~6)×10^{14} n/s [3]. Therefore, the xenon gas activation inside a fusion reactor should be considered. Second, xenon isotopes are ascribed to the transitional region below the closed neutron shell with $N = 82$ [4]. The analysis of the transitional nucleus neutron cross-section is a fundamental interest of nuclear chemists and physicists. The possibility of comparing these competing approaches raises an additional interest from the experimentalists to obtain data on even–even Xe nuclei. Particularly important are the non-yrast level properties that provide strict

Received 23 September 2021; Accepted 3 December 2021; Published online 18 February 2022
* Supported by the National Natural Science Foundation of China (11875016, 12165006)
† E-mail: luojh71@hxu.edu.cn

tests for various nuclear models [5]. Nuclear reactions can be induced *via* neutrons with an energy of approximately 14 MeV (e.g., $(n, 2n)$, (n, p), (n, α), (n, t), and (n, d) reactions [6,7]). Such reactions are essential for nuclear physics to elucidate the inertial confinement fusion (ICF) plasma [8,9]. The neutron′s energy distributed in the deuterium-tritium (DT) ICF plasma relies on the power of stopping for the corresponding tritons and deuterons. For this purpose, the cross-section values of xenon isotope nuclear reactions induced by 14 MeV neutrons are required. However, the preparation of appropriate rare-gas targets for irradiation is difficult, which explains the lack of data on the corresponding cross-sections. For the ^{124}Xe isotopes, the cross sections of the ^{124}Xe$(n,2n)^{123}$Xe reaction at approximately 14 MeV have been determined by a limited number of laboratories [10-13]. The cross-sections of the ^{126}Xe$(n, 2n)^{125}$Xe, ^{128}Xe$(n, 2n)^{127}$Xe, ^{130}Xe$(n, 2n)^{129m}$Xe, ^{132}Xe$(n, 2n)^{131m}$Xe, ^{130}Xe$(n, p)^{130}$I, ^{131}Xe$(n, p)^{131}$I, and ^{132}Xe$(n, p)^{132}$I reactions at ~14 MeV were obtained experimentally by only two groups [10, 11]. They adopted sodium perxenate ($Na_4XeO_6{\cdot}2H_2O$) and quinol-clathrates as the target sample, and the corresponding result was reported at only one energy point. In addition, significant differences have been identified among previous literature results [10-14]. These differences are mainly triggered by two factors:

1) Decay data deficiencies (characteristic γ-ray intensity). For the ^{124}Xe$(n,2n)^{123}$Xe reaction, the cross-sections were measured by Sigg and Kuroda (1976) [10] and Kondaiah *et al*. (1968) [11] with the characteristic γ-ray intensity at 63.9% and 47.3% for the same characteristic γ-ray of 148.9 keV, respectively (refer to Table 1). Ref. [12] provides no information on decay. The datum for 48.9% was recently measured [1]. For the ^{127}Xe product radionuclide, the cross-sections have also been determined by Sigg and Kuroda (1976) [10], with the characteristic γ-ray intensity at 60.8% for the same characteristic γ-ray of 202.8 keV (refer to Table 1). The data for 68.7% have been recently measured [1]. For the ^{129m}Xe product radionuclide, the cross-sections have been determined by Kondaiah *et al*. (1968) [11] using the characteristic γ-ray intensity to be 5.8% for the same characteristic γ-ray 196.56 keV. The data for 4.59% have been recently measured [1].

2) Interfering reactions. For the ^{132}Xe$(n, p)^{132}$I (β^- (100%), $T_{1/2}$=2.295 h) reaction, in previous research [10,11], the 773 keV gamma-ray emitted in the ^{132}I decay was used to obtain the values of the ^{132}Xe$(n, p)^{132}$I reac-

Table 1. Summary of cross-section measurements for $(n, 2n)$ and (n, p) reactions on xenon isotopes from previous measurements.

Reaction	Decay data	Detector	Monitor reaction	Reference
^{124}Xe$(n, 2n)^{123}$Xe	$T_{1/2}$=2.1 h, $E\gamma$=148.9 keV, $I\gamma$=63.9%	GeLi	^{27}Al$(n,\alpha)^{24}$Na	Ref. [10]
	$T_{1/2}$=2.08 h, $E\gamma$=149 keV, $I\gamma$=47.3%	GeLi	^{136}Xe$(n, 2n)^{135}$Xe	Ref. [11]
	$T_{1/2}$=2.04 h, decay data: *No information* Xenon gas enriched to 40% ^{124}Xe.	GeLi	^{27}Al$(n,\alpha)^{24}$Na	Ref. [12]
	$T_{1/2}$=2.08 h, $E\gamma$=148.92 keV, $I\gamma$=48.9%; $E\gamma$=178.02 keV, $I\gamma$=14.9% Xenon gas enriched to 99.6% ^{124}Xe.	HPGe	^{197}Au$(n, 2n)^{196}$Au	Ref. [13]
^{126}Xe$(n, 2n)^{125}$Xe	$T_{1/2}$=17 h, $E\gamma$=188.4 keV, $I\gamma$= 54.97%	GeLi	^{27}Al$(n,\alpha)^{24}$Na	Ref. [10]
	$T_{1/2}$=16.8 h, $E\gamma$=187 keV, $I\gamma$= 54.97%	GeLi	^{136}Xe$(n, 2n)^{135}$Xe	Ref. [11]
^{128}Xe$(n, 2n)^{127}$Xe	$T_{1/2}$=36.4 d, $E\gamma$=202.84 keV ($I\gamma$=60.8%), $E\gamma$=172.1 keV ($I\gamma$=20.8%), $E\gamma$=374.96 keV ($I\gamma$=18.3%)	GeLi	^{27}Al$(n,\alpha)^{24}$Na	Ref. [10]
	$T_{1/2}$=36.41 d, $E\gamma$=203 keV, $I\gamma$= 68.37%	GeLi	^{136}Xe$(n, 2n)^{135}$Xe	Ref. [11]
^{130}Xe$(n, 2n)^{129m}$Xe	$T_{1/2}$=8 d, $E\gamma$=196.5 keV, $I\gamma$= 4.59%	GeLi	^{27}Al$(n,\alpha)^{24}$Na	Ref. [10]
	$T_{1/2}$=8 d, $E\gamma$=197 keV, $I\gamma$=5.8%	GeLi	^{136}Xe$(n, 2n)^{135}$Xe	Ref. [11]
^{132}Xe$(n, 2n)^{131m}$Xe	$T_{1/2}$=11.9 d, $E\gamma$=163.9 keV, $I\gamma$= 2%	GeLi	^{27}Al$(n,\alpha)^{24}$Na	Ref. [10]
	$T_{1/2}$=11.8 d, $E\gamma$=164 keV, $I\gamma$=2.1%	GeLi	^{136}Xe$(n, 2n)^{135}$Xe	Ref. [11]
^{130}Xe$(n, p)^{130}$I	$T_{1/2}$=12.4 h, $E\gamma$=536.1 keV ($I\gamma$=100%), $E\gamma$=668.4 keV ($I\gamma$=94%), $E\gamma$=739.4 keV ($I\gamma$=81%), $E\gamma$=418.0 keV ($I\gamma$=33%),	GeLi	^{27}Al$(n,\alpha)^{24}$Na	Ref. [10]
	$T_{1/2}$=12.3 h, $E\gamma$=538 keV ($I\gamma$=99.2%), $E\gamma$=743 keV ($I\gamma$=86.7%)	GeLi	^{136}Xe$(n, 2n)^{135}$Xe	Ref. [11]
^{131}Xe$(n, p)^{131}$I	$T_{1/2}$=8.04 d, $E\gamma$=364.5 keV, $I\gamma$=82%	GeLi	^{27}Al$(n,\alpha)^{24}$Na	Ref. [10]
	$T_{1/2}$=8.05 d, $E\gamma$=364 keV, $I\gamma$=83.58%	GeLi	^{136}Xe$(n, 2n)^{135}$Xe	Ref. [11]
^{132}Xe$(n, p)^{132}$I	$T_{1/2}$=2.28 h, $E\gamma$=772.7 keV ($I\gamma$=75%), $E\gamma$=667.7 keV ($I\gamma$=98%), $E\gamma$=954.6 keV ($I\gamma$=16.7%), $E\gamma$=522.6 keV ($I\gamma$=15.6%), $E\gamma$=630.2 keV ($I\gamma$=13.5%)	GeLi	^{27}Al$(n,\alpha)^{24}$Na	Ref. [10]
	$T_{1/2}$=2.26 h, $E\gamma$=773 keV, $I\gamma$=79.81%	GeLi	^{136}Xe$(n, 2n)^{135}$Xe	Ref. [11]

tion cross section. However, the 773 keV gamma-ray did not only emerge from the ^{132}I product radionuclide, but also from the ^{132}Xe(n, p)^{132m}I (half-life $T_{1/2}$ = 1.387 h, γ-ray energy E_γ = 772.6 keV, and intensity I_γ = 14.0%) reaction, and from the ^{134}Xe(n, α)^{131m1}Te (half-life $T_{1/2}$ = 33.25 h, γ-ray energy E_γ = 773.67 keV, and intensity I_γ = 36.8%) reaction (refer to Table 1, the decay data of the daughter nucleus, the detector used, and the monitor reaction are also given).

Owing to the lack of data and differences between these data, the libraries of evaluated nuclear data rely heavily on nuclear model calculations in the 13–15 MeV energy regions; hence, large differences exist among the various evaluations. For instance, for the ^{124}Xe(n, $2n$)^{123}Xe reaction, the evaluation result of database JENDL-4.0 [15] was 1.5 times that of ENDF/B-VIII.0 [16] (CENDL-3 [17]). For the ^{130}Xe(n, p)^{130}I reaction, the result of database JENDL-4.0 [15] was 3 times that of ENDF/B-VIII.0 [16] (JEFF-3.3 [18], RUSFOND [19]). For the ^{131}Xe(n, p)^{131}I reaction, the result of database JENDL-4.0 [15] was 4 times that of ENDF/B-VIII.0 [16], JEFF-3.3 [18], RUSFOND [19], and CENDL-3 [17]. For the ^{132}Xe(n, p)^{132}I reaction, the result of database JENDL-4.0 [15] was 4 times that of RUSFOND [19]. Consequently, new measurements for the Xe(n,x) cross section are required in the 13–15 MeV neutron energy range.

This paper reports the ^{124}Xe(n, $2n$)^{123}Xe, ^{128}Xe(n, $2n$)^{127}Xe, ^{130}Xe(n, $2n$)^{129m}Xe, ^{126}Xe(n, $2n$)^{125}Xe, ^{130}Xe(n, p)^{130}I, ^{132}Xe(n, $2n$)^{131m}Xe, and ^{131}Xe(n, p)^{131}I reaction cross-section measurements at 13–15 MeV. We adopted natural high-purity pressured Xe gas as a target, and a high-resolution HPGe detector was utilized to measure the gamma activities of the product nuclei. During the irradiation process, each sample was wrapped in pure cadmium foils to circumvent the effects of the ^{124}Xe(n,γ)^{125}Xe, ^{126}Xe(n,γ)^{127}Xe, ^{128}Xe(n,γ)^{129m}Xe, and ^{130}Xe(n,γ)^{131m}Xe reactions induced by thermal neutrons on the ^{126}Xe(n,2n)^{125}Xe, ^{128}Xe(n,2n)^{127}Xe, ^{130}Xe(n,2n)^{129m}Xe, and ^{132}Xe(n,2n)^{131m}Xe reactions, respectively. The obtained results were compared and analyzed with previously reported results, the evaluation data in JENDL-4.0 [15], ENDF/B-VIII.0 [16], CENDL-3 [17], JEFF-3.3 [18], and RUSFOND [19] libraries, and the theoretical excitation curves acquired using the TALYS-1.95 [20] code.

II. EXPERIMENTAL

The procedure for radioactive product identification and cross-section measurements is outlined in a different paper [21-23]. Only the most prominent characteristics associated with the measurements conducted in this study are presented.

A. Samples and irradiation

Xenon gas (99.999% purity with natural isotopic composition) was stored in a stainless-steel sphere with a 20 mm inner diameter and 1 mm wall thickness. The xenon gas weight was obtained by subtracting the container weight from the total weight. The gas weight and pressure were 2.3–5.2 g and 120–250 atm, respectively. Five of such samples of xenon gas and 10 monitors (20 mm diameter), comprising 99.99% pure and 0.12 mm thick Nb foil and a 99.999% pure and 0.3 mm thick Al foil, were prepared for irradiation. A ZrNbAl –Xe –AlNbZr stack was prepared from these five samples and mounted at 0°, 45°, 90°, 110°, and 135° angles relative to the beam. The end of the neutron production target was 5 cm apart from the sample sphere center (see Fig. 1). The neutron fluxes for the low-threshold of the ^{130}Xe(n, p)^{130}I, ^{131}Xe(n, p)^{131}I, and ^{132}Xe(n, p)^{132}I reactons were monitored by implementing the ^{27}Al(n, α)^{24}Na reaction (E_{th} = 3.249 MeV). The neutron fluxes for the high-threshold of the ^{124}Xe(n, $2n$)^{123}Xe, ^{126}Xe(n, $2n$)^{125}Xe, ^{128}Xe(n, $2n$)^{127}Xe, ^{130}Xe(n, $2n$)^{129m}Xe, and ^{132}Xe(n, $2n$)^{131m}Xe reactions were monitored by implementing the ^{93}Nb(n, $2n$)^{92m}Nb reaction cross-section (E_{th} = 8.792 MeV). The cross-sections of the ^{27}Al(n, α)^{24}Na and ^{93}Nb(n, $2n$)^{92m}Nb monitor reactions were adopted from a different paper [24]. Subsequently, a cadmium foil (99.95% pure and 1 mm thick) was wrapped around the samples to minimize the influence of the ^{124}Xe(n, γ)^{125}Xe, ^{126}Xe(n, γ)^{127}Xe, ^{128}Xe(n, γ)^{129m}Xe, and ^{130}Xe(n, γ)^{131m}Xe reactions activated *via* thermal neutrons on the ^{126}Xe(n, $2n$)^{125}Xe, ^{128}Xe(n, $2n$)^{127}Xe, ^{130}Xe(n, $2n$)^{129m}Xe, and ^{132}Xe(n, $2n$)^{131m}Xe reactions, respectively.

The K-400 neutron generator at the Institute of Nuclear Physics and Chemistry of the China Academy of Engineering Physics was utilized to irradiate the samples for 2 h. The neutron yields were ~(4 –5)×10^{10} n/s. The ^{3}H(d,n)^{4}He reaction produced 14 MeV neutrons when excited by a 134 keV deuteron beam energy and a 200 μA beam current. The generator described above uses a solid ^{3}H–Ti target that is 2.65 mg/cm^2 thick. To monitor the neutron flux within the irradiation, the accompanying α-particles were utilized. An Au–Si surface barrier detector

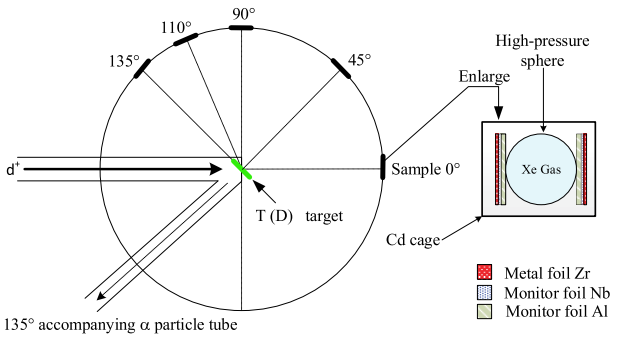

Fig. 1. (color online) Sample position with the target assembly.

was set at an angle of 135° relative to the beam direction. The obtained data were adopted for the correction of the neutron flux deviation.

B. Incident neutron energies

The average energies of neutron during the irradiating tests at the 0°, 45°, 90°,110°, and 135° incident angles were established via two approaches. The first approach adopted the cross-section ratios of the ^{93}Nb(n, $2n$)^{92m}Nb and ^{90}Zr(n, $2n$)$^{89m+g}$Zr reactions [25]. Another approach utilized the expressions obtained from Ref. [23]. The results obtained by the two approaches are consistent within their uncertainties. These neutron energies were 14.8, 14.4, 14.1, 13.8, and 13.5 MeV, respectively. The neutron energy uncertainty at 5 cm was assessed to be equal to 0.2 MeV, following the consideration of the specimen and the d^+ beam sizes (~4 mm) [25].

C. Radioactivity measurements

After irradiation, the samples decay for different amounts of time (ranging from 55 min to 5 days depending on the half-life of the daughter nucleus), and the gamma-ray activities of the ^{123}Xe, ^{125}Xe, ^{127}Xe, ^{129m}Xe, ^{131m}Xe, ^{130}I, ^{131}I, ^{24}Na, ^{92m}Nb, and ^{132}I nuclei were measured by the calibrated detector of GEM-60P HPGe (with the crystal length and diameter equal to 72.3 and 70.1 mm, respectively). The energy resolution at 1.332 MeV and a relative efficiency were equal to 1.69 keV and about 68%, respectively. The detector was calibrated using standard sources of γ-ray. Monte Carlo simulations were also performed to correct the geometry difference between the γ-ray calibration sources used for determining the efficiency of the HPGe detectors and the Xe sphere. The partial spectra of γ-ray for Xe samples collected after 4.5 h and 32.7 h irradiations are presented in Figs. 2 and 3, respectively. In addition to the strong lines of interest at 148.9 and 536.07 keV in Fig. 2 and 188.4, 202.86, 163.93, 196.56, and 364.49 keV in Fig. 3, in the former figure, the weaker ^{132}I γ-ray transitions at 522.65 keV are also indicated. The ORTEC® GammaVision® Gamma Spectrum Analysis computer program examined the peak area [26] using the emulation package of ORTEC® MAESTRO® MCA for data collection and analysis [26].

Table 2 presents the above mentioned reactions, the characteristics of the corresponding reaction product radioactive decay, and their abundance.

III. DATA PROCESSING AND RELATED EXPERIMENTAL UNCERTAINTIES

A. Experimentally determined cross-sections

The reaction cross-sections were calculated as follows [27-31]:

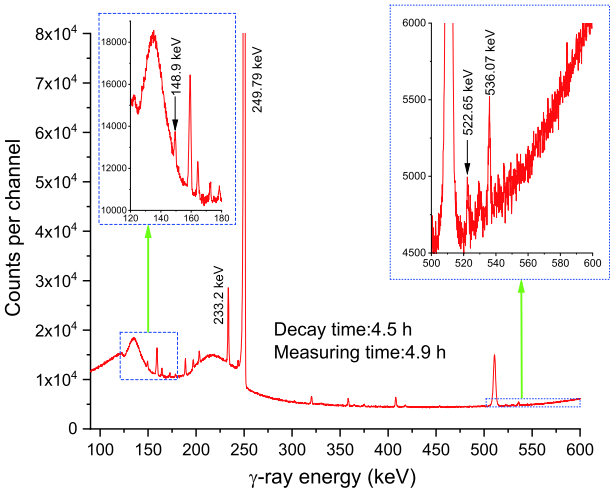

Fig. 2. (color online) γ-ray spectrum of xenon obtained with a 68% relative efficient HPGe detector at E_n=13.5 MeV, 4.5 h after the neutron activation of xenon isotopes and an acquisition time of 4.9 h. The lines of interest are 148.9, 522.6, and 536.07 keV. In the energy ranges of 120 –180 keV and 500–600 keV, the enlarged portion of the spectrum is given.

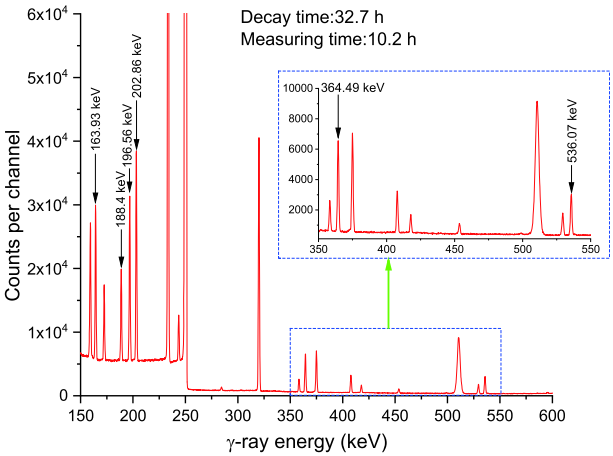

Fig. 3. (color online) γ-ray spectrum of xenon obtained with a 68% relative efficient HPGe detector at E_n=14.8 MeV, 32.7 h after the neutron activation of xenon isotopes, and an acquisition time of 10.2 h. The lines of interest are 188.4, 202.86, 163.93, 196.56, and 364.49 keV. In the energy ranges of 350–550 keV, the enlarged portion of the spectrum is given.

$$\sigma_x = \frac{[S\varepsilon I_\gamma \eta KMD]_0}{[S\varepsilon I_\gamma \eta KMD]_x} \frac{[\lambda AFC]_x}{[\lambda AFC]_0} \sigma_0, \tag{1}$$

where the subscripts *0* and *x* denote the standard monitor and measured reactions values, respectively, while F represents an activity correction factor:

$$F = f_c \times f_s \times f_g \times f_\Omega, \tag{2}$$

where f_c, f_s, f_g, and f_Ω denote the correcting factors repres-

Table 2. Reactions and decay data of the associated activation products (obtained from Ref. [1]).

Abundance of target isotope (%)	Reaction	E-threshold/MeV	Mode of decay (%)	$T_{1/2}$	$E\gamma$/keV	$I\gamma$ (%)
0.0952(3)	^{124}Xe(n, $2n$)^{123}Xe	10.569	EC(100)	2.08(2) h	148.9	48.9(6)
0.0890(2)	^{126}Xe(n, $2n$)^{125}Xe	10.105	EC(100)	16.9(2) h	188.42	53.8(3)
1.9102(8)	^{128}Xe(n, $2n$)^{127}Xe	9.686	EC(100)	39.346(3) d	202.86	68.7(12)
4.0710(13)	^{130}Xe(n, $2n$)^{129m}Xe	9.566	IT(100)	8.88(2) d	196.56	4.59(14)
26.9086(33)	^{132}Xe(n, $2n$)^{131m}Xe	9.170	IT(100)	11.84(4) d	163.93	1.95(6)
4.0710(13)	^{130}Xe(n,p)^{130}I	2.179	β^-(100)	12.36(1) h	536.07	99
21.232(30)	^{131}Xe(n,p)^{131}I	0.190	β^-(100)	8.0252(6) d	364.49	81.5(8)
26.9086(33)	^{132}Xe(n,p)^{132}I	2.814	β^-(100)	2.295(13) h	522.65	16.0(5)
100	^{27}Al(n,α)^{24}Na	3.249	β^-(100)	14.997(12) h	1368.6	100
100	^{93}Nb(n, $2n$)^{92m}Nb	8.972	EC (100)	10.15(2) d	934.44	99.15(4)

The numbers in brackets represent the uncertainties, for example, 0.0952(3) % means (0.0952±0.0003)%, while 2.08(2) h means (2.08±0.02) h.

enting the coincidence summing impact of the cascade γ-rays created by the nuclides, the self-absorption of the γ-rays, the samples counting geometries, and the solid angle of neutron flux, respectively. The calculations of the coincidence summing correction factors were based on the approach explained in previous studies [32,33].

Some of these factors were calculated by the following weighted average formula:

$$f_s = 6\int_0^1 \frac{\mu r(1-r^2)}{1-\mathrm{e}^{-2\mu\sqrt{1-r^2}}}\mathrm{d}r, \tag{3}$$

$$f_g = 3\int_0^1 \left(1+\frac{\sqrt{1-r^2}}{L}\right)^2 r\sqrt{1-r^2}\mathrm{d}r, \tag{4}$$

$$f_\Omega = \frac{\frac{1}{2}(\Omega_1+\Omega_3)}{\Omega_2}, \tag{5}$$

where μ denotes the coefficient of linear attenuation at photon energy E (see Table 2), L is the distance from the specimen to the HPGe surface, while Ω_1, Ω_2, Ω_3 represent the solid angle of the front monitor disk, sample and back monitor disks relative to the center of the target, respectively. The coefficient of mass attenuation (μ/ρ) was obtained using the γ-energy taken from a previous study [34]. The linear attenuation coefficient of natural xenon gas was determined as $\mu = \rho(\mu/\rho)$, where ρ (in g/cm^3) represents the Xe gas density in stainless-steel spheres. The linear attenuation coefficient of stainless steel was determined as $\mu = 7.86(\mu/\rho)$, where the density of iron is 7.86 g/cm^3. The comprehensive self-absorption correction factors are presented in Table 3, and the results are distributed between 1.072 and 2.014. The value of the correction factor f_Ω is 1.0756.

In the process of calculating the cross sections of the ^{130}Xe(n,2n)^{129m}Xe, ^{132}Xe(n,2n)^{131m}Xe, ^{130}Xe(n,p)^{130}I, and ^{131}Xe(n,p)^{131}I reactions, the contributions of the interfering ^{129}Xe(n, n')^{129m}Xe, ^{131}Xe(n, n')^{131m}Xe, ^{131}Xe(n, d)^{130}I, and ^{132}Xe(n, d)^{131}I reactions were respectively subtracted using the following equations [7,35]:

$$\begin{aligned}\sigma(^{\mathrm{nat}}\mathrm{Xe}(n,x)^{129m}\mathrm{Xe}) =& 0.040710\sigma(^{130}\mathrm{Xe}(n,2n)^{129m}\mathrm{Xe}) \\ &+ 0.264006\sigma(^{129}\mathrm{Xe}(n,n')^{129m}\mathrm{Xe}) \\ =& \frac{[S\varepsilon I_\gamma\eta KMD]_0}{[S\varepsilon I_\gamma KMD]_x}\frac{[\lambda AFC]_x}{[\lambda AFC]_0}\sigma_0,\end{aligned} \tag{6}$$

$$\begin{aligned}\sigma(^{\mathrm{nat}}\mathrm{Xe}(n,x)^{131m}\mathrm{Xe}) =& 0.269086\sigma(^{132}\mathrm{Xe}(n,2n)^{131m}\mathrm{Xe}) \\ &+ 0.21232\sigma(^{131}\mathrm{Xe}(n,n')^{131m}\mathrm{Xe}) \\ =& \frac{[S\varepsilon I_\gamma\eta KMD]_0}{[S\varepsilon I_\gamma KMD]_x}\frac{[\lambda AFC]_x}{[\lambda AFC]_0}\sigma_0,\end{aligned} \tag{7}$$

$$\begin{aligned}\sigma(^{\mathrm{nat}}\mathrm{Xe}(n,x)^{130}\mathrm{I}) =& 0.040710\sigma(^{130}\mathrm{Xe}(n,p)^{130}\mathrm{I}) \\ &+ 0.21232\sigma(^{131}\mathrm{Xe}(n,d)^{130}\mathrm{I}) \\ =& \frac{[S\varepsilon I_\gamma\eta KMD]_0}{[S\varepsilon I_\gamma KMD]_x}\frac{[\lambda AFC]_x}{[\lambda AFC]_0}\sigma_0,\end{aligned} \tag{8}$$

$$\begin{aligned}\sigma(^{\mathrm{nat}}\mathrm{Xe}(n,x)^{131}\mathrm{I}) =& 0.21232\sigma(^{131}\mathrm{Xe}(n,p)^{131}\mathrm{I}) \\ &+ 0.269086\sigma(^{132}\mathrm{Xe}(n,d)^{131}\mathrm{I}) \\ =& \frac{[S\varepsilon I_\gamma\eta KMD]_0}{[S\varepsilon I_\gamma KMD]_x}\frac{[\lambda AFC]_x}{[\lambda AFC]_0}\sigma_0.\end{aligned} \tag{9}$$

The interfering ^{131}Xe(n, d)^{130}I and ^{132}Xe(n, d)^{131}I reaction cross-sections were 0.09, 0.15, 0.22, 0.32, and 0.50 mb and 0.30, 0.41, 0.56, 0.80, and 1.11 mb, respectively, at 13.5, 13.8, 14.1, 14.4, and 14.8 MeV, respectively.

Table 3. Correction factors for the self-absorption of the sample at a given gamma-ray energy. The angles of the five samples relative to the beam are 0° (No. 1), 45° (No. 4), 90° (No. 2), 110° (No. 5), and 135° (No. 3), respectively.

γ-ray energy/keV	$(\mu/\rho)/(\mathrm{cm}^2/\mathrm{g})$		μ/cm^{-1}			Sample densities $\rho/(\mathrm{g/cm}^3)$	Correction factors f_s
	Fe	Xe	Fe	No.	Xe		
148.9	0.2003	0.7486	1.5740	1	0.9298	1.2420	2.014
				2	0.4385	0.5857	1.477
				3	0.8920	1.1916	1.970
				4	0.4116	0.5498	1.451
				5	0.4082	0.5453	1.447
163.93	0.1824	0.6243	1.4333	1	0.7754	1.2420	1.823
				2	0.3657	0.5857	1.396
				3	0.7439	1.1916	1.788
				4	0.3432	0.5498	1.375
				5	0.3404	0.5453	1.372
188.42	0.1577	0.4557	1.2393	1	0.5660	1.2420	1.582
				2	0.2669	0.5857	1.291
				3	0.5430	1.1916	1.558
				4	0.2506	0.5498	1.276
				5	0.2485	0.5453	1.274
196.56	0.1495	0.3997	1.1748	1	0.4964	1.2420	1.506
				2	0.2341	0.5857	1.258
				3	0.4763	1.1916	1.486
				4	0.2197	0.5498	1.245
				5	0.2179	0.5453	1.243
202.86	0.1450	0.3704	1.1394	1	0.4600	1.2420	1.467
				2	0.2169	0.5857	1.240
				3	0.4414	1.1916	1.449
				4	0.2036	0.5498	1.228
				5	0.2020	0.5453	1.227
364.49	0.0996	0.1427	0.7832	1	0.1772	1.2420	1.184
				2	0.0836	0.5857	1.106
				3	0.1700	1.1916	1.178
				4	0.0784	0.5498	1.102
				5	0.0778	0.5453	1.102
522.65	0.0825	0.0938	0.6487	3	0.1117	1.1916	1.122
				4	0.0516	0.5498	1.073
536.07	0.0816	0.0919	0.6412	1	0.1141	1.2420	1.123
				2	0.0538	0.5857	1.075
				3	0.1095	1.1916	1.120
				4	0.0505	0.5498	1.072
				5	0.0501	0.5453	1.072

These values were obtained from the interpolations performed using JEFF-3.3 [16]. The minor contributions to the activities of the product nuclei ^{130}I and ^{132}I from the interfering ^{132}Xe(n, t)^{130}I and ^{134}Xe(n, t)^{132}I reactions were neglected because their cross-sections were below 0.04 mb in the 13–15 MeV range [16]). Unfortunately, neither

the experimental measurement nor evaluated data were available for the ^{129}Xe(n, n')^{129m}Xe and ^{131}Xe(n, n')^{131m}Xe reactions. Hence, theoretical calculations were conducted to infer these data.

B. Experimental uncertainties

Our primary sources of uncertainty were the counting statistics (0.2% –22%), detector efficiency (3%), cross section of the monitor reaction (0.4% –1.5%), sample weight (0.05% –0.9%), measurements and decay times (0.1%), and the self-absorption of γ-ray (1%). Other uncertainties originated from the experimental and standard nuclear parameters, including the product nuclear half-lives (0.01% –1.1%), specific γ-ray branching ratios (0.2% – 3.1%), and target isotope abundance (0.02%–0.3%). We adopted a quadratic sum rule for the uncertainty analysis [36].

IV. CROSS-SECTION CALCULATIONS USING TALYS CODE

The cross sections of the ^{124}Xe(n, $2n$)^{123}Xe, ^{126}Xe(n, $2n$)^{125}Xe, ^{128}Xe(n, $2n$)^{127}Xe, ^{130}Xe(n, $2n$)^{129m}Xe, ^{132}Xe(n, $2n$)^{131m}Xe, ^{130}Xe(n, p)^{130}I, ^{131}Xe(n, p)^{131}I, and ^{132}Xe(n, p)^{132}I reactions were assessed by the TALYS-1.95 software [20] up to 20 MeV. TALYS-1.95 is a nuclear model code applied to replicate nuclear reactions comprising tritons, neutrons, photons, protons, deuterons, ^{3}He, and α-particles aimed at the target nuclei. It can be adopted for the reactions with incident energies up to 200 MeV [37-41]. The different parameters in the TALYS-1.95 code were adjusted according to our measured data and previous experiments conducted by other researchers for the ^{124}Xe(n,$2n$)^{123}Xe, ^{126}Xe(n,$2n$)^{125}Xe, ^{130}Xe(n,$2n$)^{129m}Xe, ^{132}Xe(n,$2n$)^{131m}Xe, ^{130}Xe(n,p)^{130}I, ^{131}Xe(n,p)^{131}I, and ^{132}Xe(n,p)^{132}I reactions.

V. RESULTS AND DISCUSSIONS

The offline γ-ray spectroscopic measuring technique was adopted to obtain cross-sections for the ^{124}Xe(n, $2n$)^{123}Xe, ^{126}Xe(n, $2n$)^{125}Xe, ^{128}Xe(n, $2n$)^{127}Xe, ^{130}Xe(n, $2n$)^{129m}Xe, ^{132}Xe(n, $2n$)^{131m}Xe, ^{130}Xe(n, p)^{130}I, ^{131}Xe(n, p)^{131}I, and ^{132}Xe(n, p)^{132}I reactions. The obtained results were then examined with those from the JENDL-4.0 [15], ENDF/B-VIII.0 [16], CENDL-3 [17], JEFF-3.3 [18], and RUSFOND [19] data libraries and TALYS-1.95 model code [20]. For the first time, this paper reports the cross-sections of several reactions (excluding the ^{124}Xe(n, $2n$)^{123}Xe and ^{132}Xe(n, p)^{132}I) at 13.5, 13.8, and 14.1 MeV (see Table 4).

Table 4. Measured cross-sections of xenon isotopes from this study compared with literature values.

Reaction	This study		Literature values		
	E_n/MeV	σ/mb	E_n/MeV	σ/mb	Reference
^{124}Xe(n,$2n$)^{123}Xe	13.5±0.2	942±96	14.6	997±80	[10]
	13.8±0.2	1017±143	14.4	1130±110	[11]
	14.1±0.2	1099±141	14.0	1436±35	[12]
	14.4±0.2	1209±156	14.4	1585±33	[12]
	14.8±0.2	1293±147	14.7	1618±33	[12]
			11.36	80.36±5.03	[13]
			11.86	228.56±12.17	[13]
			12.36	391.22±34.25	[13]
			12.85	570.07±28.46	[13]
			13.35	676.28±39.99	[13]
			13.85	793.88±38.13	[13]
			14.35	839.57±46.53	[13]
			14.8	909.44±46.87	[13]
^{126}Xe(n,$2n$)^{125}Xe	13.5±0.2	1450±117	14.6	1480±130	[10]
	13.8±0.2	1498±119	14.4	1355±165	[11]
	14.1±0.2	1620±122			
	14.4±0.2	1702±127			
	14.8±0.2	1795±113			

Continued on next page

Table 4-continued from previous page

Reaction	This study		Literature values		
	E_n/MeV	σ/mb	E_n/MeV	σ/mb	Reference
^{128}Xe(n,2n)^{127}Xe	13.5±0.2	1638±99	14.6	1752±140	[10]
	13.8±0.2	1640±99	14.4	1530±170	[11]
	14.1±0.2	1652±100			
	14.4±0.2	1696±102			
	14.8±0.2	1743±105			
^{130}Xe(n,2n)^{129m}Xe	13.5±0.2	1085±108	14.6	2031±165	[10]
	13.8±0.2	1121±113	14.4	1435±130	[11]
	14.1±0.2	1182±118			
	14.4±0.2	1242±124			
	14.8±0.2	1321±132			
^{132}Xe(n,2n)^{131m}Xe	13.5±0.2	1004±101	14.6	1000±80	[10]
	13.8±0.2	1075±107	14.4	775±65	[11]
	14.1±0.2	1085±109			
	14.4±0.2	1103±110			
	14.8±0.2	1163±116			
^{130}Xe(n,p)^{130}I	13.5±0.2	6.7±0.7	14.6	11.1±1.2	[10]
	13.8±0.2	7.0±0.8	14.4	6.7±0.8	[11]
	14.1±0.2	7.4±0.8			
	14.4±0.2	8.0±0.8			
	14.8±0.2	8.0±0.8			
^{131}Xe(n,p)^{131}I	13.5±0.2	5.5±0.6	14.6	7.0±0.8	[10]
	13.8±0.2	6.1±0.6	14.4	5.3±0.6	[11]
	14.1±0.2	6.5±0.5			
	14.4±0.2	6.7±0.5			
	14.8±0.2	7.3±0.6			
^{32}Xe(n,p)^{132}I	13.5±0.2	4.0±1.0	14.6	3.7±0.4	[10]
	14.4±0.2	4.1±1.0	14.4	2.5±0.3	[11]
Monitor reactions					
^{27}Al(n,α)^{24}Na			13.5±0.2	125.7±0.8	[24]
			13.8±0.2	123.2±0.7	[24]
			14.1±0.2	121.6±0.6	[24]
			14.4±0.2	116.8±0.4	[24]
			14.8±0.2	111.9±0.5	[24]
^{93}Nb(n,2n)^{92m}Nb			13.5±0.2	457.9±6.8	[24]
			13.8±0.2	457.9±6.8	[24]
			14.1±0.2	459.8±6.8	[24]
			14.4±0.2	459.8±6.8	[24]
			14.8±0.2	459.7±5.0	[24]

A. Reaction of ^{124}Xe(n, $2n$)^{123}Xe

For the ^{124}Xe(n, $2n$)^{123}Xe reaction, the gamma-ray with an intensity of I_γ=48.9% and 148.9 keV emitted in the decay of ^{123}Xe was utilized to obtain the cross-section of the ^{124}Xe(n, $2n$)^{123}Xe reaction. Sigg and Kuroda [10] used I_γ=63.9% while Kondaiah *et al.* [11] used I_γ=47.3% for the same ray. However, studies demonstrate that the obtained data for I_γ=48.9% exhibits higher measuring accurately. Accordingly, the cross-sections are modified as follows:

$$\sigma_{\text{corrected}} = \frac{I_{\gamma(\text{old})}}{I_{\gamma(\text{new})}}\sigma_{\text{literature}}, \tag{10}$$

where $\sigma_{\text{literature}}$ is the literature cross-section, $I_{\gamma(\text{old})}$ represents the corresponding intensity of the 148.9 keV gamma-ray in the literature, and $I_{\gamma(\text{new})}$ is 48.9%. Consequently, the divergence of the four evaluation curves given by databases JENDL-4.0 [15], ENDF/B-VIII.0 [16], CENDL-3 [17], JEFF-3.3 [18], and RUSFOND [19] is very obvious (ENDF/B-VIII.0 [16] is the same as CENDL-3 [17]). The evaluation result of database JENDL-4.0 [15] was 1.5 times that of ENDF/B-VIII.0 [16] (CENDL-3 [17]). The evaluation curves of the ENDF/B-VIII.0 [16] and CENDL-3 [17] data libraries were approximately similar to the simulated curves of excitation processed using TALYS-1.95 [20] (refer to Fig. 4). The results obtained from our measurements increase upon increasing the neutron energy in the 14 MeV range, similar to the theoretical and evaluation data. However, some differences were still observed between the results of earlier experiments. Only four laboratories have reported neutron-induced experimental cross-sections regarding the reaction of ^{124}Xe(n, $2n$)^{123}Xe [10– 13]. In the 13–15 MeV neutron region of energy, the results obtained in our study are consistent (within the experimental uncertainties) with those obtained by the TALYS-1.95 code (ldmodel 2: The back-shifted Fermi-gas model), with those obtained from the RUSFOND [19] assessments, and with the values reported by Sigg and Kuroda [10] and Kondaiah *et al.* [11]. In addition, the evaluated data obtained from JENDL-4.0 [15] and Bazan [12] exhibited larger cross-sections than those obtained from the TALYS-1.95 code (ldmodels 2 and 4), ENDF/B-VIII.0 [16] and CENDL-3 [17] assessments, and the study by Bhike *et al.* [13].

B. Reaction of ^{126}Xe(n, $2n$)^{125}Xe

For the ^{126}Xe(n, $2n$)^{125}Xe reaction, only two laboratories reported the cross section data in the previous period, and both provided only one energy point [10,11]. In this study, the ^{126}Xe(n, $2n$)^{125}Xe reaction cross-sections were determined via the ^{93}Nb(n, $2n$)^{92m}Nb monitor reaction with a high threshold. The samples were wrapped in a Cd foil to minimize the influence of the low-energy neutrons derived from ^{2}H agglomeration within the tritium target over time and background neutrons. Furthermore, the OMP parameters r_v and a_v were adjusted. Figure 5 presents the cross-sections of the ^{126}Xe(n, $2n$)^{125}Xe reaction together with calculations obtained from the TALYS-1.95 code and ENDF/B-VIII.0 [16] (RUSFOND [19]), JEFF-3.3 [18], and JENDL-4.0 [15] libraries (marked as solid lines). At 13.5 and 13.8 MeV, the data measured in this study are consistent with the assessed outcomes from the JENDL-4.0 [15] libraries, and within the limit of experimental uncertainties. In the 13-15 MeV regions, our data are higher than the literature values [10,11] (refer to Table 4 and Fig. 5), as well as the assessed outcomes obtained from the ENDF/B-VIII.0 [16] (RUSFOND [19]) and JEFF-3.3 [18] libraries, and the results of the TALYS-1.95 calculation. ENDF/B-VIII.0 [16] and RUSFOND [19] databases provide the same results. At neutron energies of 13.5, 13.8, and 14.1 MeV, our results are reported for the first time.

C. Reaction of ^{128}Xe(n, $2n$)^{127}Xe

To date, only two laboratories have experimentally

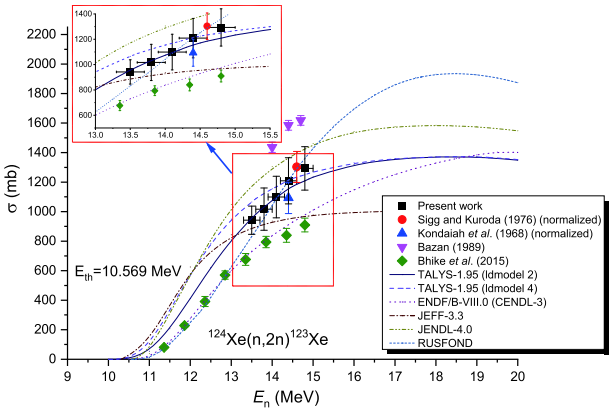

Fig. 4. (color online) Cross-section of ^{124}Xe(n,$2n$)^{123}Xe reaction.

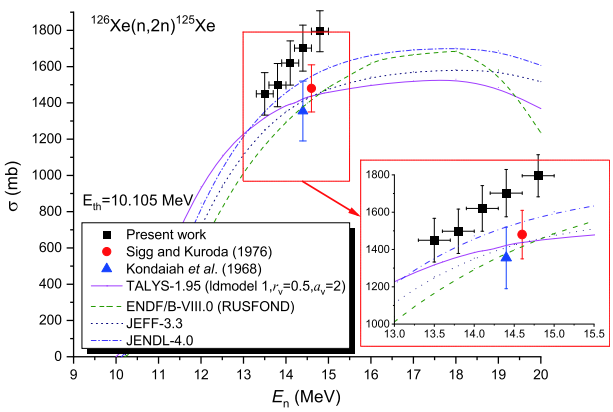

Fig. 5. (color online) Cross-section of the ^{126}Xe(n,$2n$)^{125}Xe reaction.

determined and reported the cross-sections of the ^{128}Xe(n, 2n)^{127}Xe reaction at one energy point. These values could be found in the corresponding nuclear reaction databases at 14 MeV. Early measurement [10] was carried out using the 202.8 keV (I_γ=60.8%) gamma-ray emitted in the ^{127}Xe. However, for the same ray, data for the I_γ=68.7% has been measured accurately in recent years. Hence, these literature cross sections are corrected by Eq, (10). These results provide a solid foundation to verify the reliability of the experimental results and the validity of the theoretical calculations presented here. In the theoretical calculation, the models for the r_v and a_v parameters of the optical model potential (OMP) were adjusted. The excitation curves in the ENDF/B-VIII.0 [16] (which is similar to RUSFOND [19]) and JEFF-3.3 [18] (JENDL-4.0 [15]) databases are very similar to the theoretical curves of the excitation attained *via* TALYS-1.95 [20] within the range of neutron energies with a 15 MeV threshold (refer to Fig. 6). Only minor differences among these curves can be observed. Within the limits of experimental uncertainties, the experimental data obtained here agree with the evaluation curves obtained from JEFF-3.3 [18] (JENDL-4.0 [15]) and the corrected cross-sections of Sigg and Kuroda [10], including the experiment values reported by Kondaiah *et al*. [11].

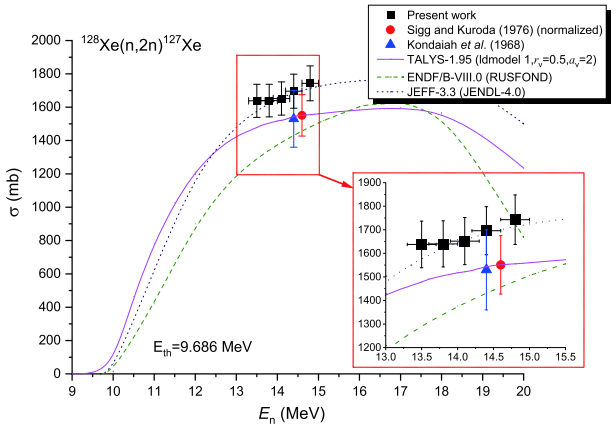

Fig. 6. (color online) Cross-section of the ^{128}Xe(n,2n)^{127}Xe reaction.

D. Reaction of ^{130}Xe(n, 2n)^{129m}Xe

The IAEA database does not contain any evaluation for the cross sections of the ^{130}Xe(n, 2n)^{129m}Xe. Only two experimental cross sections were reported for the 13.5 –14.8 MeV range [10,11], and these two reports provide the cross-sections at either 14.6 or 14.4 MeV. The OMP parameters r_v and a_v for the ^{130}Xe(n, 2n)^{129m}Xe reaction, as well as the model for the level densities, were adjusted. These cross-sections are illustrated in Fig. 7. Our data for the 13.5–14.8 MeV range disagreed with the results of experimental papers [10,11] even when considering the experimental uncertainties. From Fig. 7, it can also be observed that our values are lower than those presented in Refs. [10,11]; however, in the 13–15 MeV region, the values obtained here are higher than those obtained from the TALYS-1.95 code. Furthermore, at the energy of the 14.6 MeV, the values reported by Sigg and Kuroda [10] are approximately 1.6 times greater than the values obtained in this research. This discrepancy was very likely due to the interference of the ^{129}Xe(n, n')^{129m}Xe reaction. To date, neither experimental measurements nor evaluation results have been reported for the ^{129}Xe(n, n')^{129m}Xe reaction. However, according to the theoretical calculation findings of the TALYS-1.95 code (utilizing default parameters), the cross-section values of this reaction at 13–15 MeV are between 143 and 166 mb.

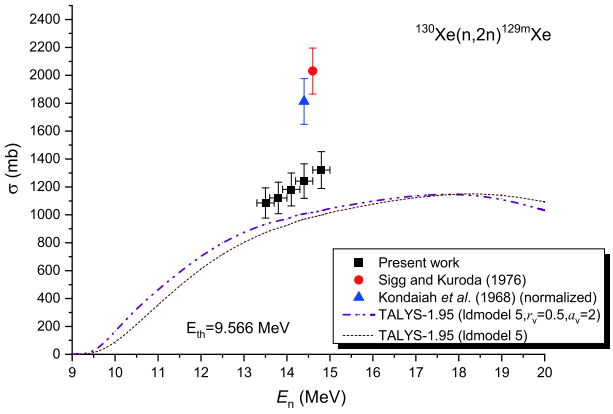

Fig. 7. (color online) Cross-section of ^{130}Xe(n,2n)^{129m}Xe reaction.

E. Reaction of ^{132}Xe(n, 2n)^{131m}Xe

For the ^{132}Xe(n, 2n)^{131m}Xe reaction, only two works [10,11] have reported cross-sections, both of which provide the cross-section data at one energy value. Although this reaction is also affected by the interfering ^{131}Xe(n, n')^{131m}Xe reaction, its impact is not as large as that of the interfering ^{129}Xe(n, n')^{129m}Xe reaction. The effect of the cross-section value of the ^{131}Xe(n, n')^{131m}Xe reaction at 13–15 MeV is 106–121 mb (theoretical results of the TALYS-1.95 with default parameters). According to Eq. (6), this value was considered in this work. Similarly, Fig. 8 presents the cross section of the ^{132}Xe(n, 2n)^{131m}Xe reaction. In addition, for the energy range between 13.3 and 15 MeV, our experimental results are in excellent agreement with the theoretical calculation (ldmodel 5: comprising microscopic level densities (Skyrme force) from Hilaire's combinatorial tables [41]) and the results obtained by Sigg and Kuroda [10] within their uncertainty limits (see Fig. 8); however, these results were larger than the experiment values reported by Kondaiah et al. [11].

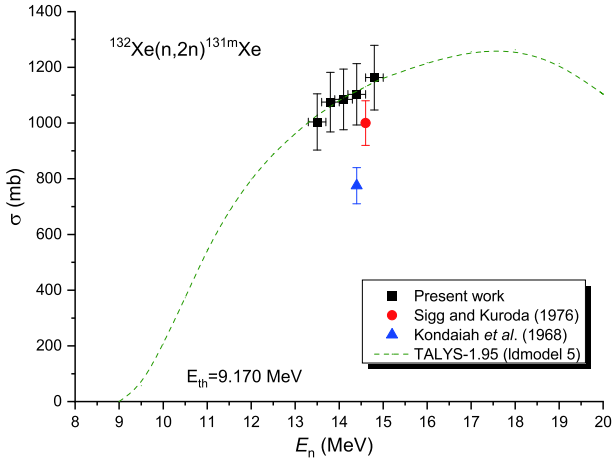

Fig. 8. (color online) Cross-section of ^{132}Xe(n,$2n$)^{131m}Xe reaction.

F. Reaction of ^{130}Xe(n, p)^{130}I

Figure 9 presents the cross sections of the ^{130}Xe(n,p)^{130}I reaction based on the results reported in [10,11]. In Fig. 9, the values obtained using the TALYS-1.95 calculations and the data obtained from the ENDF/B-VIII.0 [16] (JEFF-3.3 [18] and RUSFOND [19]) and JENDL-4.0 [15] libraries are represented in continuous lines. As illustrated in Fig. 9, there are significant dissimilarities among the results obtained from TALYS-1.95 [20], including the evaluation values acquired using JENDL-4.0 [15] at a neutron energy of approximately 14 MeV. The values evaluated by the JENDL-4.0 [15] for the ^{130}Xe(n, p)^{130}I reaction are 3 times higher those assessed by ENDF/B-VIII.0 [16], JEFF-3.3 [18], and RUSFOND [19] at a neutron energy of approximately 14 MeV. Above the 15 MeV neutron energy, in addition to becoming significantly larger, the difference between the two evaluation curves also changes in the opposite direction. The main reason for this phenomenon is the lack of necessary experimental data. Furthermore, the present result is consistent with the results reported in [11] within the limits of experimental uncertainties. At the 14.8 MeV energy point, the results obtained by Sigg and Kuroda [10] were 40% higher than those measured in this study.

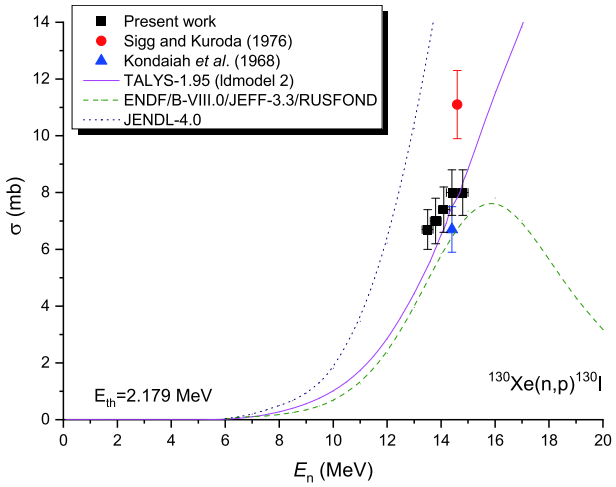

Fig. 9. (color online) Cross-section of ^{130}Xe(n,p)^{130}I reaction.

G. Reaction of ^{131}Xe(n, p)^{131}I

For the ^{131}Xe(n,p)^{131}I reaction, the following conditions were adopted for the measurements: gamma-rays at 364.49 keV ($I\gamma$ = 81.5%) emitted via ^{131}I (half-life, $T_{1/2}$ = 8.0252 d). The measurements reported in the literature adopt the same decay data as this work. Figure 10 compares our data with those of the and literature [10, 11], together with the data obtained by TALYS-1.95 and from the JENDL-4.0 [15], ENDF/B-VIII.0 [16], CENDL-3 [17], JEFF-3.3 [18], and RUSFOND [19] libraries. The agreement between these data is the best at the 13–15 MeV range (see Fig. 10), despite the lack of experimental data at an early stage. Within the neutron energy rage of 13.5–14.8 MeV, our values agree well with the experimental data obtained in [10] and with the evaluated data obtained from the CENDL-3 [17] libraries, within the limits of experimental uncertainty. However, all of our data are below those of JENDL-4.0 [15] (refer to Fig. 10), and the result of the JENDL-4.0 database [15] was 4 times that of ENDF/B-VIII.0 [16], JEFF-3.3 [18], RUSFOND [19], and CENDL-3 [17]. For the theoretical calculation of the ^{131}Xe(n, p)^{131}I reaction, although the OMP parameters r_v and a_v, as well as the level densities, were adjusted to 2, 2, and ld-model 3, respectively, the results remain slightly higher than those obtained in the present study and the evaluated data obtained from the ENDF/B-VIII.0 [16], CENDL-3 [17], JEFF-3.3 [18], and RUSFOND [19] libraries.

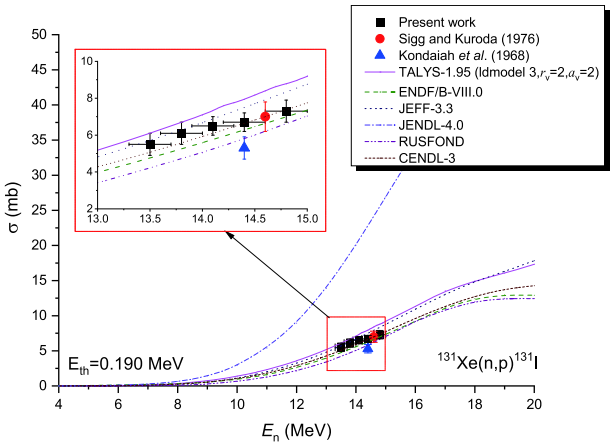

Fig. 10. (color online) Cross-section of ^{131}Xe(n,p)^{131}I reaction.

H. Reaction of ^{132}Xe(n, p)^{132}I

In this study, the latest decay data (half-life $T_{1/2}$ = 2.295 h, characteristic γ-ray energy E_γ = 522.65 keV, and γ-ray intensity I_γ = 16.0 %) of the ^{132}I product were used to deduce the cross-section value of the ^{132}Xe(n,p)^{132}I reaction. The characteristic gamma-ray energy of 773 keV was selected in [10,11] to determine the activity of the ^{132}I product. However, this line originates from both ^{132}I and also from ^{132m}I (half-life $T_{1/2}$ = 1.387 h, γ-ray energy E_γ = 772.6 keV, and intensity I_γ = 14.0 %) of the ^{132}Xe(n, p)^{132m}I reaction, including the ^{131m1}Te (half-life $T_{1/2}$ = 33.25 h, γ-ray energy E_γ = 773.67 keV, and intensity I_γ = 36.8 %) of the ^{134}Xe(n, α)^{131m1}Te reaction. The results obtained in this study are presented in Fig. 11, together with all other data from previous reports [10,11], theoretical calculation results form the TALYS-1.95 (ldmodel 2) code, and the evaluation data from the ENDF/B-VIII.0 [16], CENDL-3 [17], JEFF-3.3 [18], and RUSFOND [19] libraries. As can be observed from Fig. 11, the divergence of the three group evaluation data curves and theoretical curve is relatively large, and this difference gradually becomes larger with an increase in neutron energy. At around 14 MeV, the result of the JENDL-4.0 database [15] was 4 times that of RUSFOND [19]. In this case, the experimental results play an important role in eliminating the differences between the evaluation data and optimizing the parameters of the nuclear theoretical model.

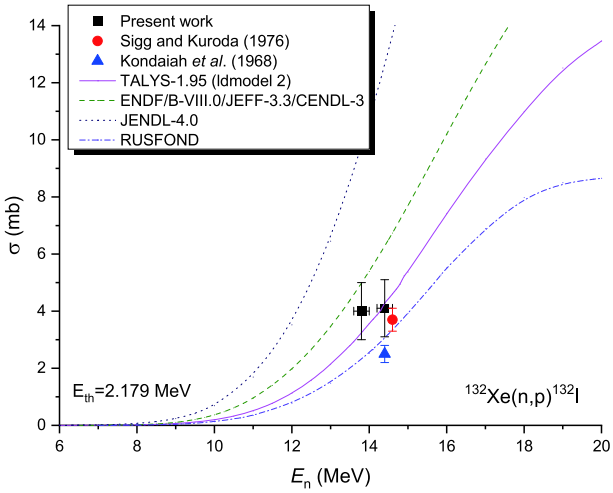

Fig. 11. (color online) Cross-section of ^{132}Xe(n,p)^{132}I reaction.

VI. CONCLUSIONS

The cross-sections of multiple reactions including ^{124}Xe(n, 2n)^{123}Xe, ^{126}Xe(n, 2n)^{125}Xe, ^{128}Xe(n, 2n)^{127}Xe, ^{130}Xe(n, 2n)^{129m}Xe, ^{132}Xe(n, 2n)^{131m}Xe, ^{130}Xe(n, p)^{130}I, ^{131}Xe(n, p)^{131}I, and ^{132}Xe(n, p)^{132}I reactions were measured for the 13–15 MeV neutron energies via the activation approach. The excitation functions for these reactions up to a neutron energy of 20 MeV were calculated by the Talys-1.95 program using adjusted parameters. The obtained results were compared with previous experiments, evaluated data, and theoretical results based on the Talys-1.95 code. In general, within the experimental uncertainties, the present cross-section values were consistent with those of previous experiments and the theoretical excitation curves at corresponding energies. Our novel achievements are expected to facilitate the quality of the neutron cross-section databases and assist possible novel evaluations of the cross sections of xenon isotopes in the incident neutron energy range from the threshold energy to 20 MeV. Moreover, reliable cross section data can play a key role in the verification of nuclear reaction models and the determination of model parameters, especially nuclear reactions for which experimental data are scarce. Evidently, for the first time, this study reports the experimental values of cross-sections at 13.5, 13.8, and 14.1 MeV for the ^{126}Xe(n, 2n)^{125}Xe, ^{128}Xe(n, 2n)^{127}Xe, ^{130}Xe(n, 2n)^{129m}Xe, ^{132}Xe(n, 2n)^{131m}Xe, ^{130}Xe(n, p)^{130}I, and ^{131}Xe(n, p)^{131}I reactions, as well as at 13.5 MeV for the ^{132}Xe(n, p)^{132}I reaction. Hence, this study addresses the limitations of the single energy of some cross section data and also broadens the energy range of neutron cross section data.

ACKNOWLEDGEMENT

We would like to thank the Intense Neutron Generator group at the China Academy of Engineering Physics for performing the irradiations.

References

[1] Evaluated Nuclear Structure Data File (ENSDF), (Last updated 2021-07-07) http://www.nndc.bnl.gov/ensdf/
[2] S. Parashari, S. Mukherjee, S. V. Suryanarayana *et al.*, Phys. Rev. C **99**, 044602 (2019)
[3] A. Ratkiewicz, L. Berzak Hopkins, D. L. Bleuel *et al.*, Rev. Sci. Instrum. **87**, 11D825 (2016)
[4] H. Jiang, Y. Zhou, Y. Lei *et al.*, Chin. Phys. C **45**, 094103 (2021)
[5] L. Goettig, Ch. Droste, A. Dygo *et al.*, Nucl. Phys. A **357**, 109 (1981)
[6] A. Gandhi, A. Sharma1, Yu. N. Kopatch *et al.*, J. Radioanal. Nucl. Chem. **322**, 89 (2019)
[7] J. Luo, L. Jiang, L. Shan *et al.*, Chin. Phys. C **44**, 114002 (2020)
[8] J. A. Frenje, R. Bionta, E. J. Bond *et al.*, Nucl. Fusion **53**, 043014 (2013)
[9] P. A. Bradley, G. P. Grim, A. C. Hayes *et al.*, Phys. Rev. C **86**, 014617 (2012)

[10] R. A. Sigg and P. K. Kuroda, Nucl. Sci. Eng. **60**, 235-238 (1976)
[11] E. Kondaiah, N. Ranakumar, and R. W. Fink, Nucl. Phys. A **120**, 337 (1968)
[12] F. Bazan, Progress Report, U. C., Lawrence Rad. Lab. (Berkeley and Livermore). **53929**, 162 (1989)
[13] M. Bhike, B. Fallin, M. E. Gooden *et al*., Phys. Rev. C **91**, 011601(R) (2015)
[14] Experimental Nuclear Reaction Data (EXFOR), Database Version of 28 June, 2021 International Atomic Energy Agency Nuclear Data Services https://nds.iaea.org/
[15] JENDL-4.0 (Japan, 2012), Evaluated Nuclear Data File (ENDF) Database Version of 2021-06-28 https://www-nds.iaea.org/exfor/endf.htm
[16] ENDF/B-VIII. 0 (USA, 2018), Evaluated Nuclear Data File (ENDF) Database Version of 2021-06-28 https://www-nds.iaea.org/exfor/endf.htm
[17] CENDL-3 (China, 2020), Evaluated Nuclear Data File (ENDF) Database Version of 2021-06-28 https://www-nds.iaea.org/exfor/endf.htm
[18] JEFF-3.3 (Europe, 2017), Evaluated Nuclear Data File (ENDF) Database Version of 2021-06-28 https://www-nds.iaea.org/exfor/endf.htm
[19] RUSFOND (Russia, 2010), Evaluated Nuclear Data File (ENDF) Database Version of 2021-06-28 https://www-nds.iaea.org/exfor/endf.htm
[20] A. Koning, S. Hilaire, and M. Duijvestijn, "TALYS-1.95, A nuclear reaction program " NRG-1755 ZG Petten, The Netherlands, 2019, http://www.talys.eu
[21] J. Luo, L. Jiang, and L. He, Phys. Rev. C **98**, 014619 (2018)
[22] J. Luo, L. Jiang, and X. Wang, Eur. Phys. A **54**, 67 (2018)
[23] J. Luo, L. Du, and J. Zhao, Nucl. Instrum. Meth. B **298**, 61 (2013)
[24] M. Wagner, H. Vonach, A. Pavlik *et al*, Physik Daten-Physics Data, Evaluation of cross sections for 14 important neutron dosimetry reactions, Fachinformationszentrum Karlsruhe, Gesellschaft für wissenschaftlich-technische Information mbH, in the Federal Republic of Germany. No. 13-5(1990) Karlsruhe
[25] V. E. Lewis and K. J. Zieba, Nucl. Instrum. Methods **174**, 141 (1980)
[26] GammaVision®-32, Gamma-Ray Spectrum Analysis and MCA Emulator, Software User's Manual, Software Version 5.3
[27] C. Zhu, J. Wang, L. Jiang *et al*., Chin. Phys. C **44**, 034001 (2020)
[28] F. Zhou, Y. Song, Y. Li *et al*., Chin. Phys. C **43**, 094001 (2019)
[29] F. Zhou, Y. Song, X. Chang *et al*., Chin. Phys. C **45**, 074101 (2021)
[30] J. Luo, L. Jiang, L. Shan *et al*., J. Phys. G: Nucl. Part. Phys. **47**, 075104 (2020)
[31] J. Luo and L. Jiang, Eur. Phys. A **56**, 125 (2020)
[32] G. J. McCallum and G. E. Coote, Nucl. Instr. Meth. **130**, 189 (1975)
[33] F. Zhou, Y. Zhang, J. Luo *et al*., HEP & NP **31**, 487 (2007)
[34] J. H. Hubbell and S. M. Seltzer, Tables of x-ray mass attenuation coefficients and mass energy-absorption coefficients from 1 keV to 20 MeV for elements Z = 1 to 92 and 48 additional substances of dosimetric interest (2004) http://physics.nist.gov/PhysRefData/XrayMassCoef/tab3.html
[35] J. Luo, F. Tuo, and X. Kong, J. Radioanal. Nucl. Chem. **288**, 143 (2011)
[36] N. Otuka, B. Lalremruata, M. U. Khandaker *et al*., Rad. Phys. Chem. **140**, 502 (2017)
[37] J. Koning and J. P. Delaroche, Nucl. Phys. A **713**, 231 (2003)
[38] C. Kalbach, Phys. Rev. C **33**, 818 (1986)
[39] P. A. Moldauer, Phys. Rev. C **14**, 764 (1976)
[40] R. Capote, M. Herman, P. Obložinský *et al*., Nucl. Data Sheets **110**, 3107 (2009)
[41] RIPL-2 Reference Input Parameter Library, IAEA, A-1400 Vienna, IAEA-NDS, retrieved from https://www-nds.iaea.org/RIPL-2/